Catalysis Science & Technology

PAPER

View Article Online
View Journal | View Issue

Cite this: *Catal. Sci. Technol.*, 2017, 7, 2252

Epoxidation of propene using Au/TiO_2: on the difference between H_2 and CO as a co-reactant†

Shamayita Kanungo,‡[a] Yaqiong Su,‡[b] M. F. Neira d'Angelo,[a] Jaap C. Schouten[a] and Emiel J. M. Hensen *[b]

Received 18th March 2017,
Accepted 19th April 2017

DOI: 10.1039/c7cy00525c

rsc.li/catalysis

The role of the reducing gas in the direct epoxidation of propene to propene oxide (PO) using O_2 over a Au/TiO_2 catalyst was studied through experiments and density functional theory calculations. It was found that PO can be obtained using both H_2 and CO as co-reactants. The yield of PO was much lower with CO than that with H_2. The role of the oxygen atoms of the titania support was studied by quantum-chemical investigations, which show that the mechanism involving CO as a co-reactant should proceed *via* surface oxygen vacancies, whereas with H_2 the well-accepted pathway involving OOH is favored. Steady-state isotopic transient kinetic analysis experiments demonstrate that support oxygen atoms are involved in PO formation when CO is used as the co-reactant.

Introduction

Propene oxide (PO) is an important bulk chemical intermediate, which finds application in the production of a wide range of commercial commodities.[1] The demand for PO is steadily growing. Unlike its homologue ethylene oxide, PO cannot be obtained directly by oxidation of the olefin with oxygen. Accordingly, alternative approaches have been developed for producing this valuable compound. Several of these processes are carried out on an industrial scale, despite some shortcomings such as the production of hazardous wastes (chlorohydrin process), the dependence on the economics of a co-product (SMPO and MTBE/PO processes), the requirement of multiple processing steps (chlorohydrin, SMPO, HPPO and cumene recycling process) and the use of an expensive reactant (HPPO process). Therefore, the one-step synthesis of PO directly from propene and O_2 remains the most coveted route.[2]

Despite the development of several catalysts for direct epoxidation of propene, the reported conversions and selectivities are poor.[3] One of the most promising approaches is to use gold nanoparticle catalysts in combination with Ti, either in the form of titania or as isolated Ti species dispersed on silica, in combination with a sacrificial reducing gas such as H_2.[4] The use of a reducing co-reactant has been found to be indispensable for obtaining reasonable conversion of propene (5–10%), while maintaining high PO selectivity (>85%). Since this discovery by Haruta *et al.*,[4] significant research efforts have been made to improve the catalyst systems. Some examples of active catalysts are gold dispersed on TS-1, Ti-SiO_2, Ti-MCM-41 and Ti-SBA-15.[5–10] An inherent drawback of this approach is the formation of an excessive amount of water by oxidation of hydrogen. Overall, the low H_2 efficiency constitutes a major economic hurdle. It has been reported that water can replace hydrogen, although propene conversion and PO selectivity then become very low.[11,12]

It is generally assumed that propene oxidation takes place at the interface between Au nanoparticles and Ti sites. Radical $^{\bullet}OOH$ (hydroperoxo) species formed on gold by the interaction of O_2 and H species are thought to be the oxidizing species that convert propene to PO.[13] Theoretical studies have contributed to this discussion by exploring different reaction pathways and reaction intermediates. Quantum-chemical calculations performed by Molina *et al.*[14] used a one-dimensional gold rod on an anatase-TiO_2 (101) slab to model Au/TiO_2. This study indicated that propene can be adsorbed with one end on the titania surface and with the other on Au. Reactive $^{\bullet}OOH$ radicals were argued to be essential for converting propene to a metallacycle C_3H_6O intermediate. A theoretical study of Delgass and co-workers on Au/TS-1 emphasized the role of gold clusters in forming H_2O_2 and the role of Ti defect sites in their reaction with propene and H_2O_2 to form the desired product.[15] In a later work, the

[a] *Laboratory of Chemical Reactor Engineering, Department of Chemical Engineering and Chemistry, Eindhoven University of Technology, P.O. Box 513, 5600 MB Eindhoven, The Netherlands*
[b] *Laboratory of Inorganic Materials Chemistry, Schuit Institute of Catalysis, Department of Chemical Engineering and Chemistry, Eindhoven University of Technology, P.O. Box 513, 5600 MB Eindhoven, The Netherlands.*
E-mail: e.j.m.hensen@tue.nl

† Electronic supplementary information (ESI) available. See DOI: 10.1039/c7cy00525c

‡ These authors contributed equally to this work.

influence of Au–Ti proximity on the reaction mechanism was studied. Based on the finding that the formation of Ti–OOH on a Au_3/Ti-defect site model was unfavorable, a concerted mechanism was proposed in which propene is adsorbed on the Au–Ti interface rather than on a Ti site.[16] Haruta *et al.*[17] proposed that electron transfer from Au to TiO_2 may lead to the formation of Ti^{3+}–O–Au^{+} species. These Ti^{3+} surface sites can activate molecular oxygen with subsequent formation of a hydroperoxo species, which reacts with propene adsorbed on Au to form PO. In summary, although the exact mechanism remains debated, it is clear that $^{\bullet}$OOH radicals and the Au–Ti interface play significant roles in the pathway towards PO formation.

A recent study by Sobolev and co-workers demonstrated that PO can also be formed when H_2 is replaced by CO, using a Au/TiO_2 catalyst.[18] An advantage of replacing H_2 with CO is that it largely suppresses the formation of propane,[19] which is an undesirable side reaction observed.[8,19,20] These authors proposed that the reaction propagates *via* oxygen vacancy formation on the titania support. They also argued that this mechanism may also be operative in the propene/oxygen/hydrogen case, which is in discord with the well-accepted mechanism involving surface hydrogen peroxide/hydroperoxo (HOOH/$^{\bullet}$OOH) species.[18,21] This discrepancy gives rise to a number of important research questions that have not been addressed yet, namely (a) what is the role of support oxygen atoms in the epoxidation of propene, (b) can one indeed replace H_2 with other reducing gases such as CO, and if so (c) what is the underlying mechanism and what role does the support play in such a mechanism. Earlier investigations into the role of the support oxygen atoms in propene epoxidation were inconclusive.[22]

In this work, we compared the direct epoxidation of propene using a Au/TiO_2 catalyst in the presence of H_2 or CO as co-reactants. Steady-state isotopic transient kinetic analysis (SSITKA) was employed to determine the role of support oxygen atoms. The experimental part of this study was complemented by density functional theory (DFT) calculations of the reaction mechanism using a model consisting of a small Au cluster supported on titania. The catalytic activity measurements show that the PO yield with CO as the co-reactant is much lower than that obtained using H_2 as the co-reactant. Similar observations were made for other catalyst compositions and under different reaction conditions. The DFT calculations explain this difference by identifying different favorable routes for the formation of PO with CO and H_2. Significantly, these data show that the O atoms of titania are involved in the catalytic cycle, a prediction corroborated by SSITKA experiments. The combined experimental and theoretical data provide new insight into the role of the co-reactant in the selective oxidation of propene to PO.

Experimental methods

Catalyst preparation

Au/TiO_2 was prepared by two different preparation methods. A catalyst denoted Au/TiO_2-NM was prepared as outlined by Nijhuis *et al.*,[22] *i.e.*, by deposition–precipitation of Au on titania. In a typical synthesis, 1 g of TiO_2 (Degussa P-25) was suspended in 50 ml of demineralized water. The pH was adjusted to ~9.5 using a 2.5 wt% ammonia solution. Then, 35.5 μl of $HAuCl_4$ (Aldrich, 17 wt% Au), diluted in 20 ml of water, was added dropwise (over 15 min) using a burette. The slurry was kept stirring for 1 h, while maintaining the pH at 9.4–9.5 by adding ammonia. Next, the solid was collected by filtration and washed three times using demineralized water. The catalyst was dried overnight at 80 °C and calcined in static air at 120 °C (5 °C min^{-1}, isothermal period = 2 h) and 400 °C (10 °C min^{-1}, isothermal period = 4 h). The resulting catalyst had an intense purple blue color.

Another catalyst, denoted Au/TiO_2-SM, was made as outlined by Sobolev and Koltunov.[18,21] A gold precursor solution was made by dissolving 71 μl of $HAuCl_4$ (Aldrich, 17 wt% Au) in 100 ml of demineralized water and heated to 70 °C. Then, 1 g of TiO_2 (Degussa P-25) was added to the solution and stirring was continued for 1 h. After collecting the solid by centrifugation, it was suspended in 50 ml of NH_4OH (4 M) and the mixture was stirred at 70 °C for 1 h. The suspension was then filtered and washed with 100 ml of demineralized water. Calcination was carried out in static air at 80 °C for 10 h, followed by 300 °C for 4 h. The catalyst had a similar appearance to Au/TiO_2-NM, but was slightly lighter in color suggestive of a lower Au uptake.

The catalyst Au/Ti–SiO_2 was made in the same way as Au/TiO_2-NM. The support was Ti grafted on commercial SiO_2 (Ti–SiO_2). The detailed support preparation can be found in the literature.[8,9]

Catalyst characterization

Transmission Electron Microscopy (TEM) was used to determine the size distribution of the Au particles in both catalysts. The TEM images were recorded using a FEI Tecnai G2 Sphera transmission electron microscope at an accelerating voltage of 200 kV. Sample preparation involved sonication of the finely ground catalyst in ethanol and application of a few drops of the suspension onto a TEM grid. The size distribution was determined by counting all visible gold particles from approximately 20 images (at least 150 gold particles in total).

The gold loading in the catalysts was analyzed by inductively coupled plasma optical emission spectroscopy (ICP-OES) using a SpectroCiros CCD spectrometer. First, *aqua regia* was added to the samples, and then these mixtures were heated under stirring for 30 min. The solutions were cooled and then dilute HF (1 : 15 by volume in water) was added, followed by filtration.

Catalytic activity measurements

Catalytic activity measurements were performed in a flow set-up equipped with an Interscience gas chromatography system (analysis time of ~5 min), containing two analysis channels with Porabond Q and Molsieve 5A columns and thermal

conductivity detectors. The catalyst was loaded into a quartz reactor tube (inner diameter = 6 mm) which was placed in a tubular oven. A typical reaction cycle was 2 h long with a regeneration step in between at 300 °C with 10 vol% O_2 in He for 1 h. In a typical test, 150 mg of catalyst was loaded into the reactor, and the total flow was adjusted to 25 ml min^{-1} (GHSV = 10 000 ml g_{cat}^{-1} h^{-1}). The catalysts were tested under two conditions, namely at $X/O_2/C_3H_6/He$ = 1 : 1 : 1 : 7 and $X/O_2/C_3H_6/He$ = 5 : 10 : 5 : 80, where X is H_2 or CO. The propylene conversion and selectivity to PO are expressed as:

$$\text{Conversion}(\%) = \frac{\text{moles of products}}{\text{moles of propene in feed}} \times 100 \quad (1)$$

$$\text{Selectivity}(\%) = \frac{\text{moles of PO}}{\text{moles of products}} \times 100 \quad (2)$$

where "products" represent the sum of stoichiometric amounts of oxygenates, which in the case of H_2 also includes CO_2. In the case of CO as the co-reactant, CO_2 is not included, as it is assumed that all CO_2 is formed as the product of the CO oxidation side reaction. This assumption is based on the observation that the rate of CO_2 formation is negligible under the given reaction conditions.[22] This makes it unlikely that CO_2 formation rates will be much higher when H_2 is replaced by CO. Further justification for this assumption is provided in the ESI.†

Steady-state isotopic transient kinetic analysis (SSITKA)

SSITKA experiments were performed in a similar way as described in the literature.[22] In brief, 0.3 g of catalyst was loaded into the reactor after dilution with SiC to maintain a uniform reaction temperature. The reactor feed was then switched to a mixture of 30 ml min^{-1} Ar, 5 ml min^{-1} propene, 5 ml min^{-1} $^{16}O_2$ and an additional 5 ml min^{-1} Ar. After reaching a steady state, the latter two flows (5 ml min^{-1} $^{16}O_2$ and 5 ml min^{-1} Ar) were replaced by 5 ml min^{-1} $^{18}O_2$ and 5 ml min^{-1} Ne. The reaction was then continued for 20 min using $^{18}O_2$. Product analysis was performed using a mass spectrometer (MS) and a gas chromatography–mass spectrometry (GC–MS) system.

Computational methods

The mechanism of propene oxidation was investigated by spin-polarized periodic DFT calculations using the Vienna *Ab Initio* Simulation Package (VASP).[23] The ion–electron interactions were represented by the projector-augmented wave (PAW) method,[24] and the electron exchange–correlation by the generalized gradient approximation (GGA) with the Perdew–Burke–Ernzerhof (PBE) exchange–correlation functional.[25] A plane-wave basis set with a cut-off energy of 400 eV was used. The Brillouin zone integration was carried out in the Γ-point for a Au_6 cluster placed on a 5 × 2 supercell of a rutile-TiO_2(110) surface containing three O–Ti–O layers, with a vacuum space of 20 Å to avoid spurious self-interactions.[26] The (110) termination is the most stable among the rutile low-index surfaces. The small 6-atom gold cluster was chosen as a model for gold nanoparticles in their interaction with the titania support. The convergence criteria for the force and the energy were set at 50 meV $Å^{-1}$ and 0.1 meV, respectively. During geometry optimization, the bottom layer was frozen, while the upper two layers were fully relaxed. All adsorbates were fully relaxed during all calculations. The DFT+U methodology (U is a Hubbard-like term describing the on-site Coulomb interactions) was used. U_{eff} was set to 4.0 eV for the Ti 3d orbital.[27] The climbing image nudged-elastic band (CI-NEB) algorithm was used to search for the minimum energy pathways.[28,29]

Results and discussion

Characterization

Fig. 1 shows representative TEM images of Au/TiO_2-NM and Au/TiO_2-SM. These images clearly show the presence of gold nanoparticles homogeneously distributed over the support. Statistical analysis shows that the average particle size and the distribution are comparable between the two catalysts. The average gold particle size is 3.4 nm for Au/TiO_2-NM, in close agreement with values reported for gold catalysts synthesized using this method.[22] The average particle size is 3.1 nm for Au/TiO_2-SM, which is slightly higher than the Au particle size reported by Sobolev and Koltunov.[21] Table 1 lists the targeted and analyzed Au content as determined by ICP-OES. For the TiO_2-NM support, the actual Au loading is close to the targeted loading. For Au/TiO_2-SM, the actual Au loading is lower than the targeted loading.

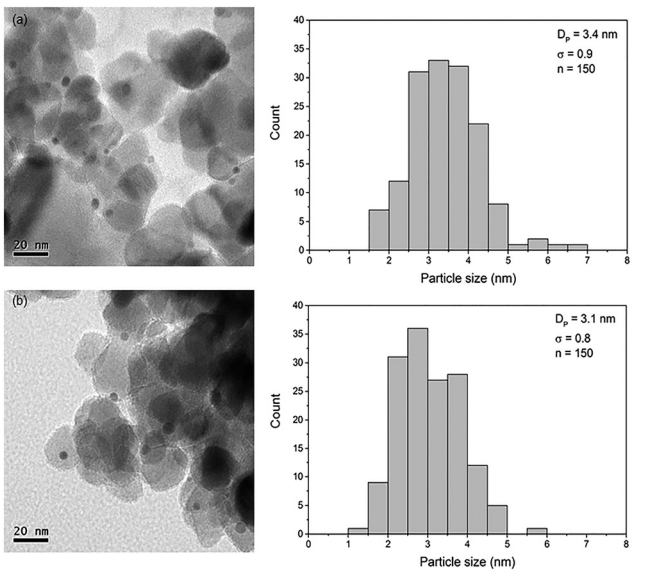

Fig. 1 TEM images of (a) Au/TiO_2-NM and (b) Au/TiO_2-SM along with the corresponding particle size distribution, showing the average particle size with standard deviation and the total number of particles counted.

Table 1 ICP-OES and TEM of Au/TiO_2 catalysts

Catalyst	Au loading, wt% (target)	Au loading,[a] wt% (real)	Particle size[b] (nm)
Au/TiO_2-NM	1	0.94	3.4 ± 0.9
Au/TiO_2-SM	2	0.60	3.1 ± 0.8

[a] Determined by ICP-OES. [b] Determined by TEM.

Catalytic activity measurements

The performance of Au/TiO_2-NM and Au/TiO_2-SM in propene epoxidation was evaluated using a gas feed composed of either $H_2/O_2/C_3H_6$ or $CO/O_2/C_3H_6$. The reaction conditions were a temperature of 50 °C, a GHSV of 10 000 mL g_{cat}^{-1} h^{-1} and a volumetric feed composition of H_2 (or CO)/O_2/C_3H_6/He = 1/1/1/7. The catalyst prepared as outlined by Sobolev and Koltunov[21] was also tested at 70 °C, a GHSV of 6000 mL g_{cat}^{-1} h^{-1}, and a volumetric feed composition of H_2 (or CO)/O_2/C_3H_6/He = 5 : 10 : 5 : 80 for reasons of comparison to literature data.[18,21]

Fig. 2 and 3 show the performance in terms of the rate of formation of PO with time on stream of Au/TiO_2-NM and Au/TiO_2-SM, respectively. For both catalysts, the rate of PO formation is higher when H_2 is used as the reducing gas in comparison with CO. With time on stream, the catalysts display initially increasing activity followed by a sharp decline, which is typical for titania-supported gold catalysts used in propene oxidation.[30] The maximum PO yield using H_2 for Au/TiO_2-NM is 1.6% (~20 g_{PO} kg_{cat}^{-1} h^{-1}) and the selectivity to PO is higher than 99%, which is in good accordance with the literature.[4] When CO is used in place of H_2, the maximum yield obtained is 0.6% (~14 g_{PO} kg_{cat}^{-1} h^{-1}) with similarly high PO selectivity. It should be mentioned here that CO_2 was excluded from the conversion and selectivity data when CO was the co-reactant. This is based on the assumption that CO_2 is the product of CO oxidation rather than a full combustion product from propene. Water is the undesired by-product of combustion of the H_2 co-reactant. The rates of H_2O and CO_2 formation for both co-reactants are shown in Fig. 4. These data trend with time on stream in the same way as the PO formation rate, suggesting that the active sites for PO formation and co-reactant combustion are similar. Water is primarily formed by the undesired oxidation of hydrogen at Au sites.[2,4,8] Au/TiO_2 is a known catalyst for CO oxidation to CO_2, so it is reasonable to argue that the majority of the CO_2 product stems from the oxidation of CO at Au sites.[26,31,32] There are strong indications that the Au–TiO_2 interface plays an important role in catalyzing CO oxidation.[26,33] In both cases, the co-reactant efficiency, defined as the ratio of PO to CO_2 or H_2O, is around 20–25%.

The strong deactivation observed for both catalysts has been extensively studied in the past and is attributed to the strong adsorption of reaction products on the catalyst surface, possibly involving subsequent oligomerization.[30,34] The activity can be fully recovered by treating the catalysts in 10 vol% O_2/He at 300 °C for 1 h. This regeneration is effective for catalysts operated with either H_2 or CO as a co-reactant. This may indicate that the deactivation mechanism for both cases is the same.

The present results are at odds with those of Sobolev and Koltunov,[18,21] who reported higher PO yields when CO was the co-reactant. The present data show that PO is formed when CO is the co-reactant, but the activity is substantially lower in comparison with that obtained using H_2 as the co-reactant. To ensure that the slightly different reaction

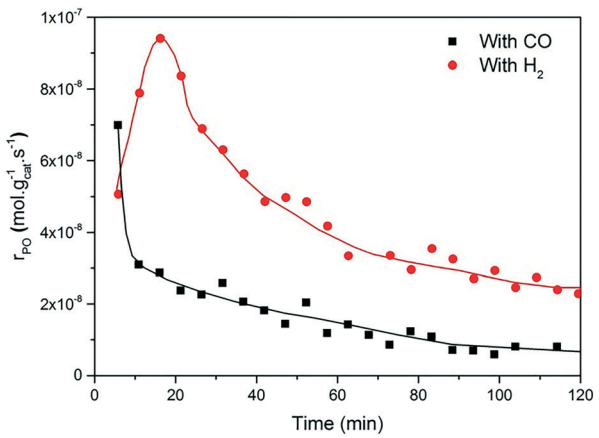

Fig. 2 Time-on-stream formation rate of PO during a 2 h catalytic test over Au/TiO_2-NM at X/O_2/C_3H_6/He = 1 : 1 : 1 : 7, where X = CO (black box) and H_2 (red circles), at 50 °C and GHSV = 10 000 mL g_{cat}^{-1} h^{-1} (N.B.: 1 × 10^{-7} mol g_{cat}^{-1} s^{-1} corresponds to 20.9 g_{PO} kg_{cat}^{-1} h^{-1}; solid lines are drawn to guide the eye).

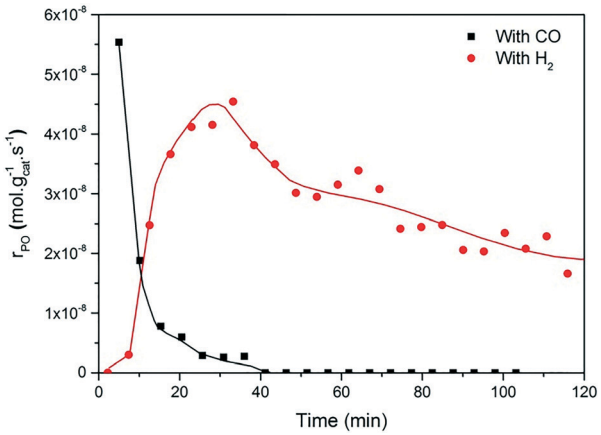

Fig. 3 Time-on-stream formation rate of PO during a 2 h catalytic test over Au/TiO_2-SM at X/O_2/C_3H_6/He = 1 : 1 : 1 : 7, where X = CO (black box) and H_2 (red circles), at 50 °C and GHSV = 10 000 mL g_{cat}^{-1} h^{-1}.

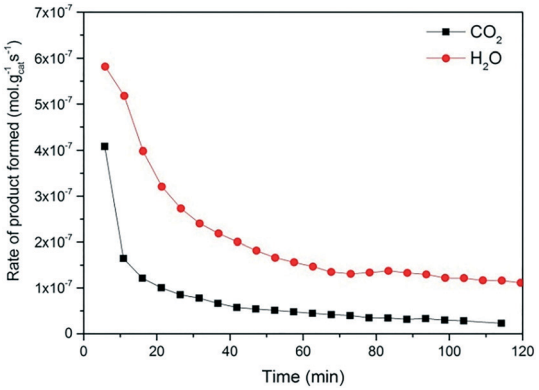

Fig. 4 Time-on-stream formation rates of CO_2 and water during a 2 h catalytic test over Au/TiO_2-NM at X/O_2/C_3H_6/He = 1 : 1 : 1 : 7, where X = CO (black box) and H_2 (red circles); temp = 50 °C and GHSV = 10 000 mL g_{cat}^{-1} h^{-1}.

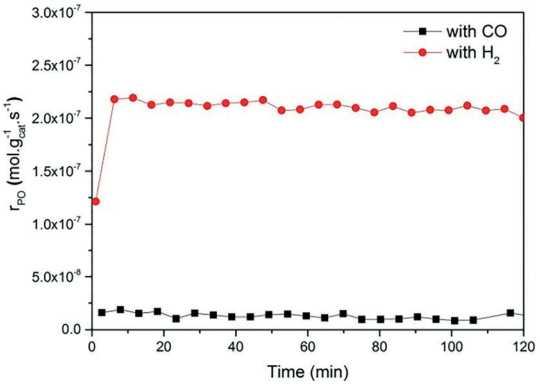

Fig. 6 Time-on-stream formation rate of PO during a 2 h catalytic test over 0.1% Au/Ti–SiO_2 at X/O_2/C_3H_6/He = 1 : 1 : 1 : 7, where X = CO (black box) and H_2 (red circles), at 200 °C and GHSV = 10 000 mL g_{cat}^{-1} h^{-1}.

conditions do not cause this difference, we evaluated the catalytic performance of Au/TiO_2-SM, the same catalyst explored by Sobolev and Koltunov, under the same conditions. The results shown in Fig. 5 confirm that the PO formation rates are lower with CO than those with H_2. Deactivation is more pronounced in this case and the PO formation rate drops to negligible values after about 1 h.

We noted that the Au loading in our case was lower than that reported in the literature.[21] Therefore, we prepared a 2 wt% Au-loaded catalyst (Au/TiO_2-NM) by deposition–precipitation as this method ensures complete uptake of the gold in the solution. The resulting performance of this catalyst with CO and H_2 (ESI†) confirmed that H_2 is the preferred co-reactant. Finally, as it is also known that catalysts based on Ti sites dispersed on silica as the support for gold exhibit more stable and active catalytic performance, we compared the performance of 0.1% Au/Ti–SiO_2 in both reactions (Fig. 6). We found that the PO formation rates were stable and significantly higher with H_2 as the co-reactant.

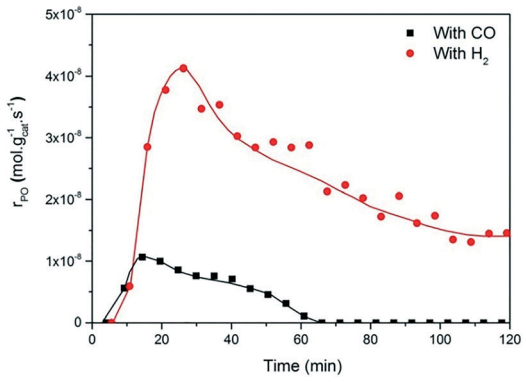

Fig. 5 Time-on-stream formation rate of PO during a 2 h catalytic test over Au/TiO_2-SM at X/O_2/C_3H_6/He = 5 : 10 : 5 : 80, where X = CO (black box) and H_2 (red circles), at 70 °C and GHSV = 6000 mL g_{cat}^{-1} h^{-1}, the same conditions used by Sobolev and Koltunov.[18]

Computational modeling

Adsorption of C_3H_6 and O_2. Fig. 7a shows the surface model consisting of a Au_6 cluster placed on the (110) surface of rutile TiO_2. Two Ti^{4+} ions are reduced to Ti^{3+} due to electron transfer from the Au_6 cluster to TiO_2(110).[35] The two reduced Ti ions are in the second Ti layer of the support.[36] We verified the existence of Ti^{3+} ions by determining the spin magnetic moment of all Ti atoms in the unit cell. In this way, we identified the presence of two Ti centers with a 3d spin magnetic moment of 0.83 μ_B, indicative of the localization of an unpaired localized electron in the 3d orbital. Fig. 8a depicts the iso-surface of the spin density, highlighting the presence of two Ti^{3+} ions. We first examined candidate adsorption sites of propylene and oxygen at the Au_6/TiO_2(110) interface. Adsorption of C_3H_6 *via* the double bond onto a single Au atom is much stronger (−176 kJ mol^{-1}) than bridged adsorption *via* two neighbouring Au atoms (−94 kJ mol^{-1}) (Fig. 7b). Metiu *et al.* reported that C_3H_6 adsorption is much

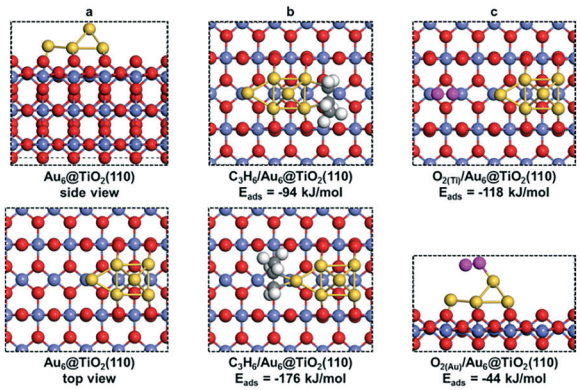

Fig. 7 (a) Side (above) and top (below) views of Au_6@TiO_2(110). (b) C_3H_6 adsorbed on dual Au atoms (above) and single Au atom (below) at the Au_6@TiO_2(110) interface. (c) O_2 adsorbed on exposed Ti atoms (above) and supported Au_6 cluster (below) at the Au_6@TiO_2(110) interface. Color code: red, titania surface oxygen; pink, oxygen of adsorbed O_2; grey, carbon; yellow, Au; blue, Ti; white, hydrogen.

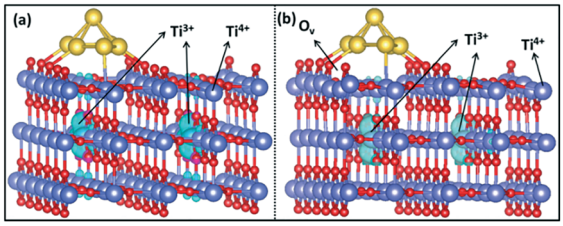

Fig. 8 The spin-density iso-surface (in light blue) of Ti^{3+} cations in (a) intact Au_6@TiO_2(110) and (b) defective Au_6@TiO_2(110) with one oxygen vacancy.

stronger on a single Au atom of a positively charged Au_5^+ cluster (−170 kJ mol^{-1}) than that on a single Au atom of a neutral Au_5 cluster (−122 kJ mol^{-1}).[37] The former binding energy is close to our result and the development of a positive charge on the gold cluster is due to the reduction of the support. O_2 prefers to adsorb on Ti Lewis acid sites with an adsorption energy of −118 kJ mol^{-1}. The adsorption energy of O_2 on Au is only −44 kJ mol^{-1} (Fig. 7c). After O_2 adsorption on a Ti Lewis acid site, the spin magnetic moment of all Ti atoms is 0.00 μ_B, showing that the electrons initially present in the 3d orbital of the two Ti centers have been transferred to the O_2 adsorbate. The disappearance of the two Ti^{3+} ions and the elongation of the O–O bond of Ti-adsorbed O_2 to 1.41 Å show that O_2 has a superoxide O_2^{2-} character.[38,39]

Oxygen vacancy formation. To explore the role of the co-reactant, we investigated the reaction of surface oxygen atoms of the titania support with H_2 and CO at the interface between the Au_6 cluster and the TiO_2(110) surface. Molecular hydrogen is strongly adsorbed on the interfacial Au atom with an energy of −117 kJ mol^{-1}. Its dissociation is almost barrierless (ESI†), suggesting that the adsorption of hydrogen will be dissociative. Water formation involves a relatively high activation barrier of 69 kJ mol^{-1} and is endothermic (ΔE = 61 kJ mol^{-1}) *via* reaction of the initially formed OH groups on titania with Au–H (ESI†). Water desorption, which results in an oxygen vacancy, costs 123 kJ mol^{-1}. Such a vacancy can also be obtained by oxidation with CO. In this case, adsorption of CO takes place on a surface Ti site with an energy of −55 kJ mol^{-1}, which is consistent with the reported values on TiO_2.[40,41] CO can also adsorb on coordinatively unsaturated Au sites, and the adsorption energy is weaker than −1.00 eV.[42] We argue that these sites should be covered by propene because of its much stronger binding to these Au sites. The Ti-adsorbed CO can react with a surface oxygen at the Au_6/TiO_2(110) interface, resulting in an oxygen vacancy. The barrier to form CO_2 is only 55 kJ mol^{-1}, and this process is exothermic by 36 kJ mol^{-1}. As the CO_2 molecule binds only weakly to the surface, the recombinative desorption step is endothermic (ΔE = 42 kJ mol^{-1}). We found that this reaction can also proceed without the Au cluster with a lower barrier of 22 kJ mol^{-1}. These values show that surface oxygen vacancy formation is much easier with CO than that with H_2. Accordingly, we explored the mechanisms of PO formation for two cases, *i.e.*, (i) through the formation of a surface oxygen vacancy with CO as the co-reactant and (ii) without such a surface vacancy with H_2 as the co-reactant.

Propene epoxidation over Au_6/TiO_2(110) without a co-reactant. We first explored the reaction pathways without the presence of co-reactants (Fig. 9). The adsorption energies of propene on the Au_6 cluster and of O_2 between two adjacent Ti sites are −176 kJ mol^{-1} and −118 kJ mol^{-1}, respectively. The excess electrons of titania transfer to adsorbed O_2, resulting in the formation of an O_2^{2-} species in which the O–O bond is pre-activated. The formation of PO overcomes an energy barrier of 107 kJ mol^{-1}, being exothermic by 76 kJ mol^{-1}. In the transition state for PO formation, the O–O and C_1–O bond lengths are 1.74 Å and 1.83 Å, respectively; those between Au and C_1 and C_2 are 2.67 Å and 2.18 Å, respectively. Following PO desorption which costs 122 kJ mol^{-1}, one oxygen atom is left behind. In the next step, another propene adsorbs on the Au cluster (E_{ads} = −147 kJ mol^{-1}) and reacts with this leftover O to form another PO; this process overcomes an energy barrier of 87 kJ mol^{-1}. Desorption of the second PO molecule costs 137 kJ mol^{-1}.

Propene epoxidation over Au_6/TiO_2(110) with H_2. In the pathway involving H_2 (Fig. 9), we explored H_2 dissociation on Au and O_2 adsorbed between two Lewis acid Ti sites. We started from the surface model with propene adsorbed on the interfacial Au site. Formation of ˙OOH and a bridging ˙OH species in this way involves an energy barrier of 69 kJ mol^{-1}. This reaction is strongly exothermic (ΔE = −198 kJ mol^{-1}). The O atom of the OOH species then reacts with the C=C double bond of the adsorbed propene, involving a barrier of 63 kJ mol^{-1} (TS2), resulting in the formation of an OH group on the surface. Desorption of PO costs 137 kJ mol^{-1} and the adsorbed OH intermediate reacts with the acidic OH group to form water (barrier of 14 kJ mol^{-1}). The reaction cycle ends by the desorption of water (ΔE = 112 kJ mol^{-1}).

It is interesting to compare the transition states for PO formation involving OOH and O_2 (see the ESI†). In the former case, the C_1–O bond is substantially longer and the C_1–Au bond is shorter than those in the O_2-assisted pathway. In the transition state TS2, the O–O and C_1–O bond lengths are 1.74 and 2.00 Å, and the Au–C_1 and Au–C_2 bond lengths are 2.47 and 2.20 Å. In the transition state TS1′ for PO formation, the O–O and C_1–O bond lengths are 1.74 Å and 1.83 Å, respectively; those between Au and C_1 and C_2 are 2.67 Å and 2.18 Å, respectively. The O–O bond length of ˙OOH is 1.46 Å, which is longer than that of adsorbed O_2 (1.41 Å), demonstrating that the O–O bond becomes weakened after hydrogenation. Moreover, one OH˙ species is left after the reaction of ˙OOH with propene, while one isolated oxygen is left on the surface without H_2. The presence of hydrogen stabilizes the isolated oxygen atom.

As mentioned earlier, two Ti^{3+} ions are present in the Au_6/TiO_2(110) model (Fig. 8a). When O_2 is adsorbed, the Ti^{3+} ions are reoxidized to Ti^{4+} and the adsorbed O_2 molecule becomes negatively charged, obtaining a superoxide character. H_2 adsorption and dissociation will reduce two Ti^{4+} into Ti^{3+} ions again and generate the OOH^- anion involved in propylene

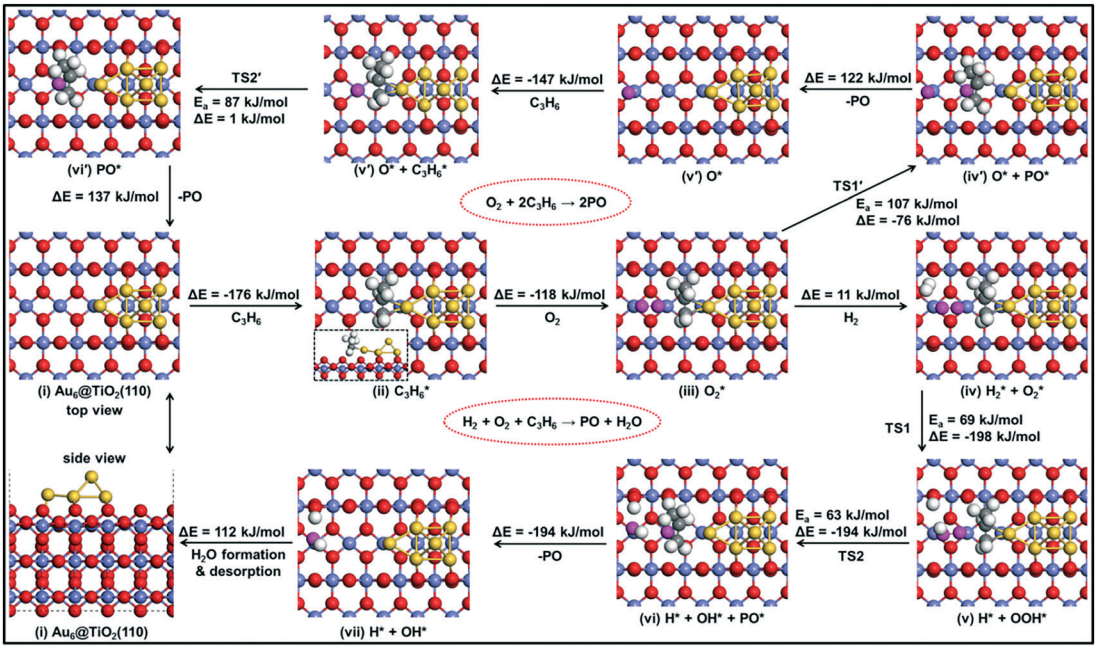

Fig. 9 The reaction energy diagram with elementary reaction steps for the epoxidation of propylene to propylene oxide (PO) using an O_2 molecule with or without H_2 assistance.

epoxidation. Obviously, the Ti^{3+} cation plays an important role in the overall reaction, which increases the reducibility of the support surface and catalyzes the O_2^{2-}/OOH^- anion formation for subsequent propene epoxidation.

Propene epoxidation over Au_6/TiO_2(110) with CO. For the reaction involving CO, we explored a reaction cycle with an oxygen vacancy in the titania surface (Fig. 10). Molecular oxygen adsorbs strongly on the oxygen vacancy. Adsorption of propene on the interfacial Au atom is slightly less favorable (E_{ads} = −122 kJ mol^{-1}) than adsorption on the model without a surface vacancy. The PO precursor is formed by dissociation of the O_2 molecule, resulting in its coordination to Au and the C_2 atom of propene. The barrier for this concerted process is 83 kJ mol^{-1} and the reaction is strongly exothermic (ΔE = −144 kJ mol^{-1}). The PO precursor is an oxometallacycle intermediate. The formation of PO occurs by coordination of the O atom to a Lewis acid Ti site, which is 79 kJ mol^{-1} more stable than the precursor. Desorption of PO costs 145 kJ mol^{-1} and the surface returns to its initial state.

It is useful to compare the energy barriers to alternative mechanisms involving only titania or gold. Molina *et al.* reported a barrier of ~150 kJ mol^{-1} for PO formation on titania.[43] Another study focusing on gold itself showed that adsorption of molecular oxygen is weak (E_{ads} > −20 kJ mol^{-1}) and the barrier for PO formation *via* the $^{\bullet}OOH$ radical is ~95 kJ mol^{-1}.[44] Both of these mechanisms are more difficult than that of the reaction explored by our group at the Au–TiO_2 interface. Accordingly, the present results emphasize the important role of the Au–Ti interface, in line with experimental data.

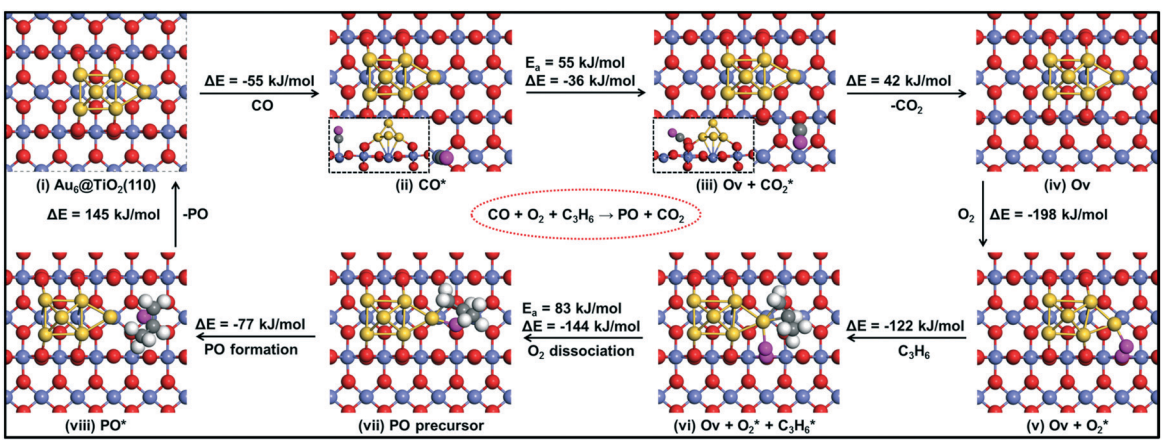

Fig. 10 The reaction energy diagram with elementary reaction steps for the epoxidation of propylene to propylene oxide (PO) using a CO molecule.

We summarize the DFT calculations by comparing the different pathways without and with co-reactants. In the absence of a co-reactant, the activation barrier for PO formation is 107 kJ mol^{-1}, while the involvement of OOH* due to the presence of H_2 lowers this activation energy to 63 kJ mol^{-1}. When CO is used as the co-reactant, the mechanism proceeds *via* a surface oxygen vacancy and the corresponding activation energy is found to be 83 kJ mol^{-1}. We observe that these trends are in good agreement with the experimental findings, where PO is not reported to be formed in the absence of a sacrificial agent on Au–Ti catalysts,[1–3] and the PO yield in the CO-assisted epoxidation of propene is much lower than that in its hydro-epoxidation, as also revealed by the catalytic performance data in the present study.

SSITKA

From the catalytic experiments, we established that CO can be used as an alternative co-reactant in the direct epoxidation of propene, while DFT calculations for this reaction revealed that support oxygen plays a crucial role in the reaction mechanism towards PO formation. To explore the role of support oxygen experimentally, SSITKA studies were carried out by switching $^{16}O_2$ with $^{18}O_2$ under steady-state reaction conditions.

Scheme 1 shows the mechanism of PO formation with CO as the co-reactant, as proposed by DFT calculations and the most likely surface species present in the SSITKA experiment. The product stream is expected to predominantly consist of $C_3H_6{}^{18}O$ (PO^{18}), $C^{16}O^{18}O$ and $C^{16}O_2$. $C^{18}O_2$ is expected as a combustion product of PO^{18} and to be present only in small amounts given the low PO yield.

Fig. 11 shows the transients for CO_2 isotopomers during epoxidation with CO, after switching from $^{16}O_2$ to $^{18}O_2$. All three CO_2 isotopomers are observed and their relative concentrations at the (pseudo) steady state are $C^{16}O_2 : C^{16}O^{18}O : C^{18}O_2 \sim 9:6:1$. That is to say, the predominant product is $C^{16}O_2$ and it is still seen 15 min after the isotopic switch, indicating the contribution of the support surface oxygen atoms to the reaction mechanism. If the O atoms of the support were not involved, we would expect the predominant product to be $C^{16}O^{18}O$, with the $C^{16}O_2$ concentration dropping to negligible levels within a very short time after the switch. Nevertheless, it can be argued that some of the formed $C^{16}O^{18}O$ exchanges with surface oxygen to give $C^{16}O_2$. This was for instance observed in a SSITKA study of CO oxidation on Au/TiO_2, but the relative amount of $C^{16}O_2$ was much lower with a $C^{16}O_2 : C^{16}O^{18}O : C^{18}O_2$ ratio of ~1 : 2 : 1.[31,32] Hence, even upon considering some exchange with support oxygen, it is highly unlikely that $C^{16}O_2$ would be the predominant product. Based on these observations, we infer that the steady release of $C^{16}O_2$ is due to the reaction of $C^{16}O$ with support oxygen, $(^{16}O)_s$ as described in eqn (3.2) (Scheme 1). It must be noted that the amount of PO was too low to be quantified accurately in the SSITKA experiments and therefore is not shown here. Qualitatively, however, it can be said that PO^{18} was observed as soon as the switch was made, which is in agreement with Scheme 1.

Conclusions

The present study explores the role of co-reactants in the direct epoxidation of propene to PO on Au/TiO_2 catalysts, using experimental and theoretical tools. When H_2 was substituted by CO as a co-reactant, PO formation was observed but with lower PO yields. PO selectivity, on the other hand, was >99% in both cases and catalyst deactivation, which is a common feature on Au/TiO_2, was also observed in the case of CO, with time on stream.

$$C^{16}O + \Delta \rightarrow C^{16}O\,\Delta \quad (3.1)$$

$$C^{16}O\,\Delta + (^{16}O)_S \rightarrow C^{16}O_2\,\Delta + ()_V \quad (3.2)$$

$$C_3H_6 + * \rightarrow C_3H_6* \quad (3.3)$$

$$C_3H_6* + {}^{16}O_2 + ()_V \rightarrow C_3H_6{}^{16}O* + (^{16}O)_S \quad (3.4)$$

When labelled oxygen is used, along with eq (3.2), the following takes place:

$$C_3H_6* + {}^{18}O_2 + ()_V \rightarrow C_3H_6{}^{18}O* + (^{18}O)_S \quad (3.6)$$

$$C^{16}O\,\Delta + (^{18}O)_S \rightarrow C^{16}O^{18}O\Delta + ()_V \quad (3.7)$$

where:

Δ:	Ti site where CO is adsorbed,
*:	Au active site where propene is adsorbed,
$(^{16}O)_S$:	Support oxygen
$()_V$:	Vacant site formed when surface oxygen has been removed

Scheme 1 Surface species expected, before and after isotopic switch, in the direct epoxidation of propene with CO.

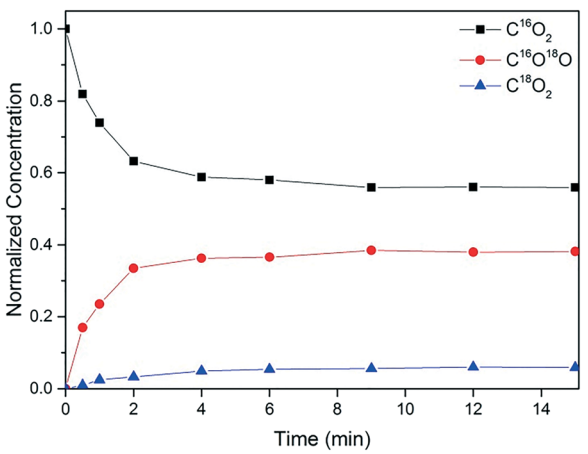

Fig. 11 SSITKA transients for the switch from $^{16}O_2$ to $^{18}O_2$ (at t = 0) after performing propene epoxidation over the Au/TiO_2-NM catalyst at 60 °C for 10 min (GHSV = 10 000 mL g_{cat}^{-1} h^{-1}, 10 vol% CO, O_2 and propene in Ar/Ne). Isotopic fractions for the products are given normalized to the amount of all isotopic varieties of the product produced at that moment.

DFT calculations were employed to explore the probable reaction mechanism for CO-assisted epoxidation and to obtain further insight into the role of support oxygen en route to PO formation. These calculations revealed that formation of oxygen vacancies on the support is energetically more feasible using CO, as compared to H_2. Hence, PO formation with CO as the co-reactant was calculated *via* this route and the resulting activation energy was 83 kJ mol^{-1}. It was also found that epoxidation without the use of any sacrificial agent on Au/TiO_2 is energetically highly demanding (107 kJ mol^{-1}) and hence improbable. The use of H_2 was found to redirect the mechanism through OOH radical formation, which subsequently lowered the activation energy to 63 kJ mol^{-1} – the lowest among the three pathways explored. Accordingly, the theoretical findings are in agreement with the experimental observations where the PO yield was observed to be the highest in hydro-epoxidation, followed by CO-assisted epoxidation, and negligible in the absence of any reducing gas. Furthermore, isotopic (SSITKA) measurements experimentally revealed the role of support oxygen in the case of CO epoxidation. This study provides valuable fundamental insight into the important role of a co-reactant in the direct epoxidation of propene and the corresponding mechanisms leading to PO formation on Au–Ti catalysts.

Acknowledgements

We acknowledge financial support for the research from The Netherlands Organization for Scientific Research (NWO) through project number 10017587, a VICI grant and Nuffic funding. Supercomputing facilities were funded by the NWO.

References

1 T. A. Nijhuis, M. Makkee, J. A. Moulijn and B. M. Weckhuysen, *Ind. Eng. Chem. Res.*, 2006, **45**(10), 3447–3459.
2 J. Huang and M. Haruta, *Res. Chem. Intermed.*, 2012, **38**(1), 1–24.
3 J. R. Monnier, *Appl. Catal.*, 2001, **221**, 73–91.
4 T. Hayashi, K. Tanaka and M. Haruta, *J. Catal.*, 1998, **178**(2), 566–575.
5 X. Feng, N. Sheng, Y. Liu, X. Chen, D. Chen, C. Yang and X. Zhou, *ACS Catal.*, 2017, **7**(4), 2668–2675.
6 X. Feng, Y. Liu, Y. Li, C. Yang and D. Chen, *AIChE J.*, 2016, **62**(11), 3963–3972.
7 W. S. Lee, M. Cem Akatay, E. A. Stach, F. H. Ribeiro and W. Nicholas Delgass, *J. Catal.*, 2012, **287**, 178–189.
8 S. Kanungo, D. M. Perez Ferrandez, F. Neira d'Angelo, J. C. Schouten and T. A. Nijhuis, *J. Catal.*, 2016, **338**, 284–294.
9 S. Kanungo, K. S. Keshri, A. J. F. van Hoof, M. F. N. d'Angelo, J. C. Schouten, T. A. Nijhuis, E. J. M. Hensen and B. Chowdhury, *J. Catal.*, 2016, **344**, 434–444.
10 C. H. Liu, Y. Guan, E. J. M. Hensen, J. F. Lee and C. M. Yang, *J. Catal.*, 2011, **282**(1), 94–102.
11 M. Ojeda and E. Iglesia, *Chem. Commun.*, 2009, 352–354.
12 J. Huang, T. Akita, J. Faye, T. Fujitani, T. Takei and M. Haruta, *Angew. Chem., Int. Ed.*, 2009, **48**(42), 7862–7866.
13 C. Sivadinarayana, T. V. Choudhary, L. L. Daemen, J. Eckert and D. W. Goodman, *J. Am. Chem. Soc.*, 2004, **126**(1), 38–39.
14 S. Lee, L. M. Molina, M. J. López, J. A. Alonso, B. Hammer, B. Lee, S. Seifert, R. E. Winans, J. W. Elam, M. J. Pellin and S. Vajda, *Angew. Chem., Int. Ed.*, 2009, **48**(8), 1467–1471.
15 D. H. Wells, W. N. Delgass and K. T. Thomson, *J. Am. Chem. Soc.*, 2004, **126**(9), 2956–2962.
16 A. M. Joshi, W. N. Delgass and K. T. Thomson, *J. Phys. Chem. C*, 2007, **765**, 7841–7844.
17 A. K. Sinha, S. Seelan, S. Tsubota and M. Haruta, *Top. Catal.*, 2004, **29**(3/4), 95–102.
18 V. I. Sobolev and K. Y. Koltunov, *Catal. Commun.*, 2013, **40**, 103–105.
19 J. Chen, S. J. A. Halin, D. M. Perez Ferrandez, J. C. Schouten and T. A. Nijhuis, *J. Catal.*, 2012, **285**(1), 324–327.
20 C. Qi, J. Huang, S. Bao, H. Su, T. Akita and M. Haruta, *J. Catal.*, 2011, **281**, 12–20.
21 V. I. Sobolev and K. Y. Koltunov, *Appl. Catal., A*, 2014, **476**, 197–203.
22 T. A. Nijhuis, E. Sacaliuc-Parvulescu, N. S. Govender, J. C. Schouten and B. M. Weckhuysen, *J. Catal.*, 2009, **265**(2), 161–169.
23 G. Kresse and J. Hafner, *Phys. Rev. B: Condens. Matter Mater. Phys.*, 1994, **49**(20), 14251–14269.
24 P. E. Blöchl, *Phys. Rev. B: Condens. Matter Mater. Phys.*, 1994, **50**(24), 17953–17979.
25 J. P. Perdew, K. Burke and M. Ernzerhof, *Phys. Rev. Lett.*, 1996, **77**(18), 3865–3868.
26 L. M. Molina, M. D. Rasmussen and B. Hammer, *J. Chem. Phys.*, 2004, **120**(16), 7673–7680.
27 K. Liu, A. Litke, Y. Su, B. G. van Campenhout, E. A. Pidko and E. J. M. Hensen, *Chem. Commun.*, 2016, **1**(Table 1), 2–5.
28 G. Henkelman and H. Jónsson, *J. Chem. Phys.*, 2000, **113**(22), 9978–9985.
29 D. Sheppard, R. Terrell and G. Henkelman, *J. Chem. Phys.*, 2008, **128**(13), 134106.
30 T. A. Nijhuis, T. Q. Gardner and B. M. Weckhuysen, *J. Catal.*, 2005, **236**(1), 153–163.
31 H. Liu, A. I. Kozlov, A. P. Kozlova, T. Shido, K. Asakura and Y. Iwasawa, *J. Catal.*, 1999, **185**(3), 252–264.
32 J. T. Calla and R. J. Davis, *J. Catal.*, 2006, **241**(2), 407–416.
33 I. X. Green, W. Tang, M. Neurock and J. T. Yates, *Science*, 2011, **333**, 736–739.
34 A. Ruiz, B. van der Linden, M. Makkee and G. Mul, *J. Catal.*, 2009, **266**(2), 286–290.
35 M. F. Camellone, J. Zhao, L. Jin, Y. Wang, M. Muhler and D. Marx, *Angew. Chem., Int. Ed.*, 2013, **52**(22), 5780–5784.
36 N. A. Deskins, R. Rousseau and M. Dupuis, *J. Phys. Chem. C*, 2011, **115**(15), 7562–7572.
37 S. Chrétien, M. S. Gordon and H. Metiu, *J. Chem. Phys.*, 2004, **121**(8), 3756–3766.
38 H. Li, H. Wang, X. Gong, Y. Guo, Y. Guo, G. Lu and P. Hu, *Phys. Rev. B: Condens. Matter Mater. Phys.*, 2009, **79**, 193401.

39 M. Huang and S. Fabris, *Phys. Rev. B: Condens. Matter Mater. Phys.*, 2007, **75**, 081404(R).
40 A. Linsebigler, G. Lu and J. T. Yates, *J. Chem. Phys.*, 1995, **103**(21), 9438–9443.
41 S. Derrouiche, P. Gravejat and D. Bianchi, *J. Am. Chem. Soc.*, 2004, **126**(40), 13010–13015.
42 Y. Wang, Y. Yoon, V. Glezakou, J. Li and R. Rousseau, *J. Am. Chem. Soc.*, 2013, **135**(29), 10673–10683.
43 S. Lee, L. M. Molina, M. J. López, J. A. Alonso, B. Hammer, B. Lee, S. Seifert, R. E. Winans, J. W. Elam and M. J. Pellin, *Angew. Chem.*, 2009, **121**, 1495–1499.
44 C. Chang, Y. Wang and J. Li, *Nano Res.*, 2011, **4**, 131–142.